Journal of the Korean Ceramic Society
Vol. 44, No. 11, pp. 597~606, 2007.

Review

Synthesis of Forsterite with High Q and Near Zero TC_f for Microwave/Millimeterwave Dielectrics

Hitoshi OHSATO†, Minato ANDO, and Tsutomu TSUNOOKA

Nagoya Institute of Technology, Gokiso-cho, Showa-ku, Nagoya 466-8555, JAPAN
(Received September 28, 2007; Accepted October 24, 2007)

ABSTRACT

With the advent of ubiquitous age, the high quality dielectric materials have been required for the wireless communications available to the millimeterwave as well as microwave frequencies. The utilizable region for the frequency has been expanding to the millimeter-wave region because of the shortage of radio frequency (RF) resources. These high frequencies would be expected for ultra high speed LAN, ETS and car anti-collision system on the intelligent transport system (ITS) and so on. Silicates are good candidates for microwave/millimeterwave dielectrics, because of their low dielectric constant ε_r and high quality factor (High Q). Forsterite (Mg_2SiO_4) is one of the silicates with low ε_r of 6.8 and $Q \cdot f$ of 240000 GHz.
In this paper, we reviewed following three categories for synthesis of forsterite:
(1) Synthesis of high Q forsterite
(2) Adjust the temperature coefficient of resonant frequency TC_f
(3) Diffusion of SiO_4- and Mg-ions on the formation of forsterite

Key words : Forsterite, Microwave/millimeterwave dielectrics, Raw materials, Diffusion of Si and Mg-ions

1. Introduction

Recently, the wireless communications have been tremendously developed.[1] The utilizable frequency region has been expanded to millimeterwaves because of shortage of conventional frequency regions. For the ultra high frequencies of millimeterwaves, the dielectrics with ultra high quality factor Q and low dielectric constant ε_r are desired. The direction of development of microwave dielectric materials are shown in Fig.1, in which quality factors $Q \cdot f$ are shown as a function of dielectric constants ε_r.[3] Curve in the figure shows an outline the upper limit of $Q \cdot f$ obtained up to now for a given ε_r. Here, $Q \cdot f$ and ε_r are two of the three important dielectric properties. Q being inversing of the dielectric loss $\tan\delta$ is desirable high. The loss is brought from polarity change due to electromagnetic wave. The effect of ε_r in shortening the wavelength is described by the relation $\lambda = \lambda_0/\varepsilon_r^{1/2}$. In the microwave region, the wave length is expected to be short due to large ε_r for miniaturization of mobile equipments. In the millimeterwave region, the ε_r value is expected small because of none need for miniaturization and reducing time delay T_{PD}.[3] The time delay (T_{PD}) is shown as following equation (1)[2]:

$$T_{PD} = \sqrt{\varepsilon_r}/c \qquad (1)$$

where, c is the velocity of light. The T_{PD} are shown as a function of ε_r in Fig. 2. Temperature coefficients of resonant frequency τ_f are also one of the three important properties. TC_f is expected to be close to near zero ppm/°C. Properties demanded on wireless communications are high ε_r for the 1st direction, high Q and high ε_r for the 2nd one and extremely high Q and low ε_r for the 3rd one. The first direction is mainly on demand for miniaturization of mobile phone parts.[5-7] The second one is on demand for increasing signal/noise ratio for the main application in mobile phone base stations.[8-10] The third direction is for devise working in millimeter-wave range.[11,12]

Silicates for candidate of millimeterwave materials have low dielectric constant, because of silica-oxygen tetrahedra composed of half covalent bonds as shown in Fig. 3.[3,4] Forsterite Mg_2SiO_4 is one of the silicates with low dielectric constant ε_r, which are expected for a good candidate of the millimeterwave dielectrics.[5] In this paper, our research for forsterite is summarized in the following categories.

(1) Synthesis of high Q forsterite.[6,7]
(2) Adjust the temperature coefficient of resonant frequency TC_f.[8,9]
(3) Diffusion of SiO_4- and Mg-ions on the formation of forsterite.[10]

2. Experimental

In this study, high purity forsterite (section 3.1 and 3.3) and rutile doped forsterite (section 3.2) were synthesized by

†Corresponding author : Hitoshi OHSATO
E-mail : ohsato.hitoshi@nitech.ac.jp
Tel : +81-52-735-5284 Fax : +81-52-735-5284

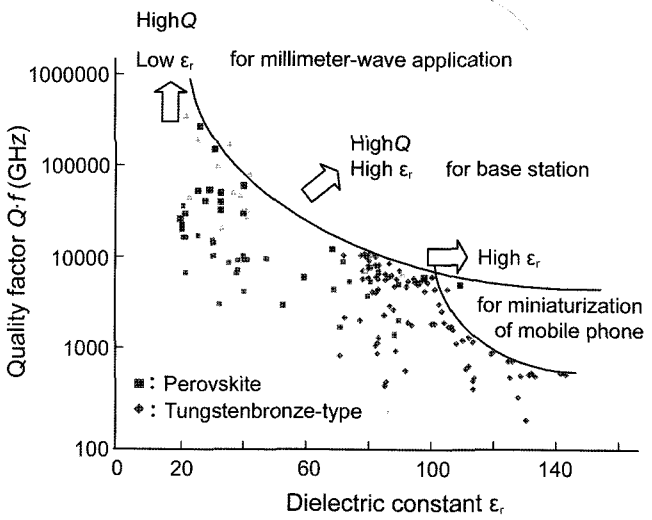

Fig. 1. Three directions of R&D of microwave dielectrics. $Q \cdot f$ are shown as a function of ε_r.

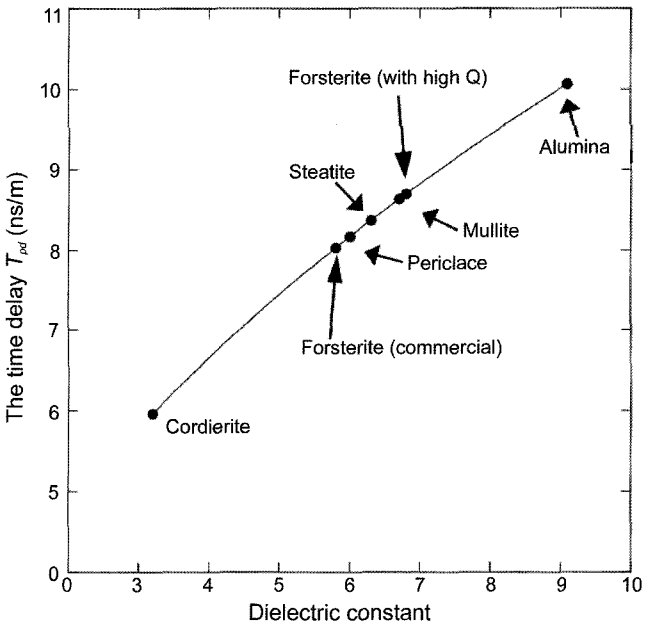

Fig. 2. Time delay (T_{PD}) as a function of dielectric constant.

conventional solid state reaction method. The raw materials with high purity more than 99% were used. Magnesia powder as follows was used through the whole synthesis: the high purity (99.99%) MgO powders with 0.08 to 0.1 μm diameter and large specific surface area of 2,600 m^2kg^{-1}, which are manufactured by gas phase oxidation process of magnesium. Silica powders were used different ones in each case: in the section 3.1, two kinds of high purity SiO_2 powders, high purity (99.8%) SiO_2 (A) with 0.82 μm diameter and specific surface area of 4000 $m^2kg^{-1}$and SiO_2 (B) with 0.8 μm diameter and specific surface area of 3800 m^2kg^{-1}. In the section 3.2, SiO_2 (99.9%) with 0.82 μm diameter was used. In the section 3.3, silica A (quartz SiO_2 with 99.8% purity and grain size of 0.82 μm), and silica B (spherical amorphous SiO_2 with 99.9% purity and grain size of 0.25 μm) were used. And high purity (99.5%) rutile TiO_2 was used in the section 3.2. These powders were mixed by ball-milling for 24 h. After the slurry was dried and calcined, the calcined powder was ball-milled again for 24 h. And the slurry was dried and smashed in mortar by pestle and sieved through 300 μm opening. Test pellets of 12 mm ϕ diameter ×6 mm thickness were formed by mechanical pressing under 8 MPa and then by cold isostatic pressing (CIP) under 200 MPa, and was sintered in a electric furnace in air.

The crystal phases were identified by X-ray powder diffraction (XRPD) using CuKa radiation. Microwave dielectric properties were measured by Hakki-Coleman's method[11,12] in the $TE_{01\delta}$ mode using network-analyzer (HP-8757, Agilent). The TC_f was measured in the temperature range between 20 and 80°C. Microstructure of sintered specimens was photographed by scanning electron microscope (SEM). Densities of the sample were measured by the Archimedes' method.

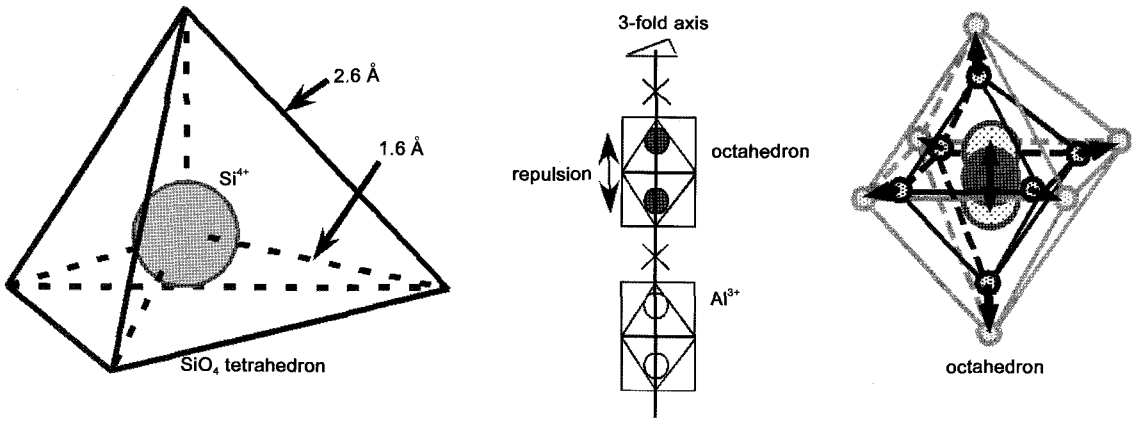

Fig. 3. Dielectric constants due to crystal structure; SiO_4 tetrahedron (a), octahedron of alumina (b), and TiO_6 octahedron (c).

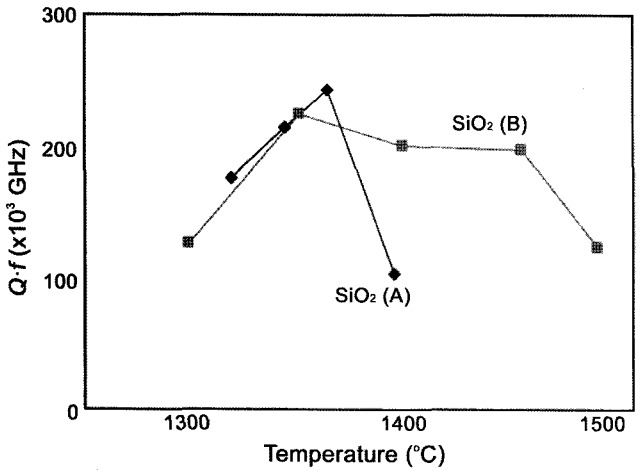

Fig. 4. Quality factor $Q \cdot f$ of forsterite ceramics using high purity raw materials silica A (A) and B (B) as a function of sintering temperature.

3. Results and Discussion

3.1. Synthesized High Q forsterite

Quality factor $Q \cdot f$ of forsterite synthesized using high purity SiO_2 (A) and (B) raw materials were shown in Fig. 4. These values were higher than 200000 GHz at the frequency of 23 GHz. The highest $Q \cdot f$ values using SiO_2 (A) and (B) raw materials were 240000 and 220000 GHz, respectively. The former showed higher value than the latter one based on the single forsterite phase as shown in Fig. 5(b). The latter was degraded by the enstatite $MgSiO_3$ precipitated as secondary phase as shown in Fig. 5(b). The calcined powder of latter at 1150°C for 3 h contains unreacted quartz and magnesia as shown in Fig. 5(a). The raw SiO_2 material of the latter is high purity but low reactivity. Precipitation of the enstatite degrades the $Q \cdot f$ value.

Table 1. Dielectric, Resistivity and Thermal Properties of Commercial Forsterite Ceramics and High Purity Forsterite Ceramics Sintered at 1360°C for 2 h

Properties	Commercial	High purity
ε_r (23 GHz)	6.5~6.6	6.8
$\tan\delta$ (23 GHz)	$8.4 \sim 17 \times 10^{-4}$	0.96×10^{-4}
Volume resistivity (Ωm) 100°C	5.0×10^{11}	8.5×10^{12}
300°C	7.0×10^{9}	1.8×10^{10}
500°C	1.0×10^{9}	4.4×10^{8}
Coefficient of thermal expansion (ppm/°C)	25~700°C 11.2	25~700°C 9.4
Thermal conductivity (w/m°C) at Room temperature	3.2	9.1

Forsterite ceramics synthesized using high purity raw materials were compared with commercial ones in Table 1. The quality factors $Q \cdot f$ for the synthesized high purity forsterite ceramics were higher than $Q \cdot f$ of 27000-13000 GHz for commercial one as shown in Fig. 6. The synthesized forsterite was single phase with high relative density of 96 to 98% as mentioned above.[6,7]

Microstructure of commercial available forsterite and that of high-purity one are shown in Fig. 7(a) and (b), respectively. The dielectric losses of commercial one was lead by much glassy phase among grains as seen in Fig. 7(a). On the other hand, synthesized forsterite ceramics has fine grain boundary which lead to low dielectric losses. In the texture of the grain boundaries, different configurations of grains were observed. The grains of commercial one has many facets of crystal surface accompanied by much-glassy phase in grain boundaries. The grains with facets, called as euhedral in crystallography, appeared as results of crystal growth in liquid phase which was introduced by impurity. The liquid phase remained as glassy phase as shown in Fig. 7(a). High

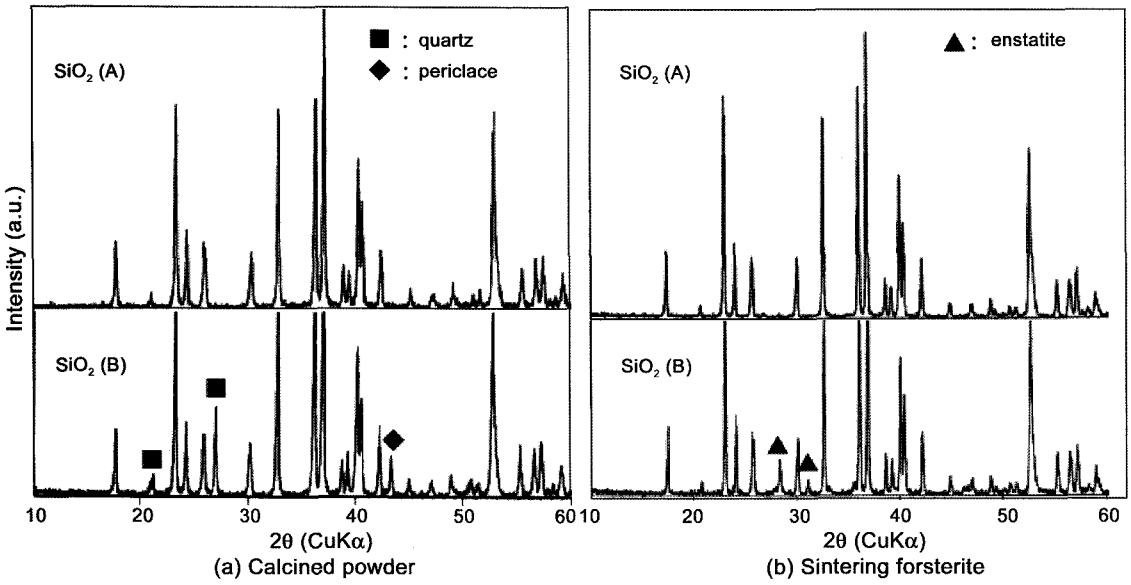

Fig. 5. XRPD patterns of calcined powders (a) and sintered ceramics (b) using SiO_2 (A) and (B).

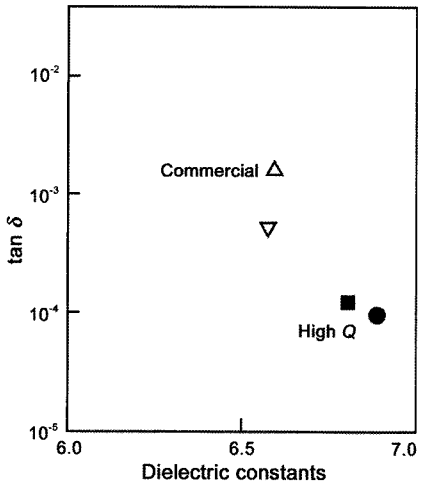

Fig. 6. Dielectric losses of commercial forsterite ceramics and high Q forsterite ceramics against dielectric constants.

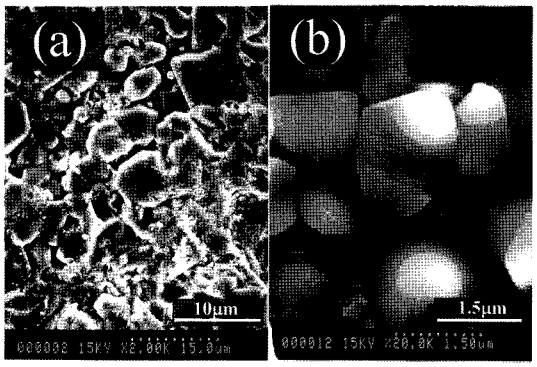

Fig. 7. SEM photographs of commercial forsterite ceramics (a) and high purity forsterite ceramics (b) sintered at 1360°C.

purity forsterite ceramics has grains without facets, called anhedral, which may be due to direct contact of grains. In Table 1, the volume resistivity of commercial forsterite ceramics is lower than that of high purity one, depend on the glassy phase. Thermal conductivity is about three times that of the commercial grade.

3.2. Adjust the temperature coefficient of resonant frequency

Forsterite with large negative temperature coefficient of resonant frequency TC_f of −65 ppm/°C was designed to be TC_f ppm/°C adding rutile with large positive TC_f of 450 ppm/°C. Fig. 8(a) and (b) show the apparent density, and TC_f and TC_ε (temperature coefficient of dielectric constant) as a function of sintering temperature and the amount of rutile, respectively. It was found that the rutile have a role of sintering aid by 100°C for addition of 0.5 to 10 wt% rutile, though the TC_f was not developed to near zero ppm/°C. The reason of non improvement of TC_f was clarified based on the phase diagram as shown in Fig. 9.[21] As the compositions of forsterite added rutile locate in the compositional triangle Mg_2SiO_4-$MgTi_2O_5$-$MgSiO_3$, rutile reacts with forsterite to make $MgTi_2O_5$ and enstatite as following chemical reaction:

$$Mg_2SiO_4 + 2TiO_2 \rightarrow MgTi_2O_5 + MgSiO_3$$

The reduction of rutile by the reaction brings large negative TC_f.

Fig. 10(a) shows the apparent density of the forsterite ceramics added 30 wt% of rutile as a function of the sintering temperature from 1200 to 1400°C. It was also found that the apparent densities keep high values of about 3.3 g/cm^3 in the samples sintered at temperatures from 1350 to 1200°C. This result indicates that it seems to be sintered even at 1200°C. Namely, rutile acts as a sintering aid for increasing sinterability of forsterite. The addition of 30 wt% of rutile reduced sintering temperature by 200°C from 1400°C for plain forsterite to 1200°C. The TC_f maintains plus 12.7 ppm/°C for the sample sintered at 1200°C as shown in Fig. 10(d), which has never been obtained up to the present. The positive value is obtained by the residual rutile with the large posi-

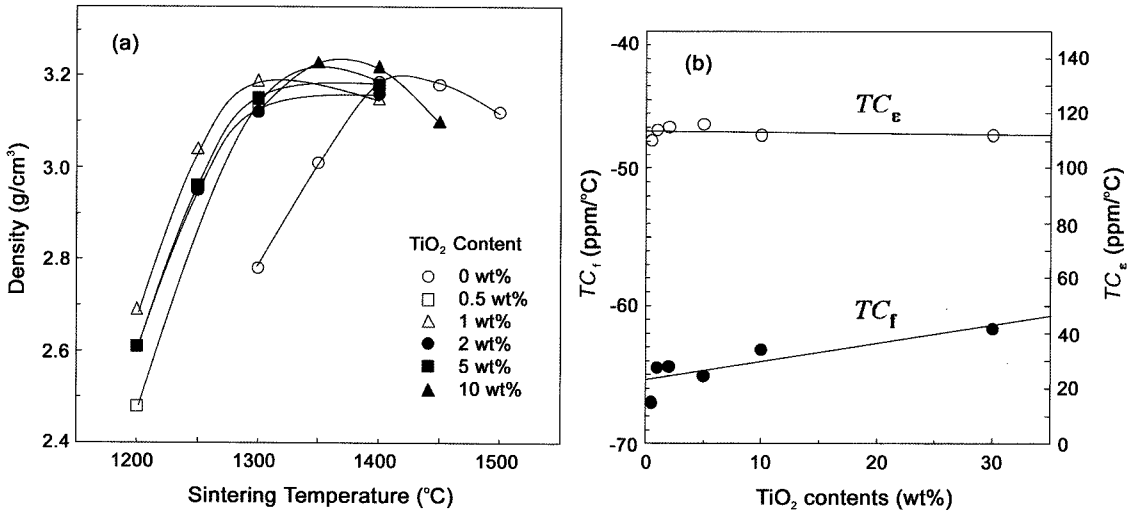

Fig. 8. Apparent density of rutile doped forsterite (a) and TC_f and TC_ε (b), as a function of sintering temperature and rutile content, respectively.

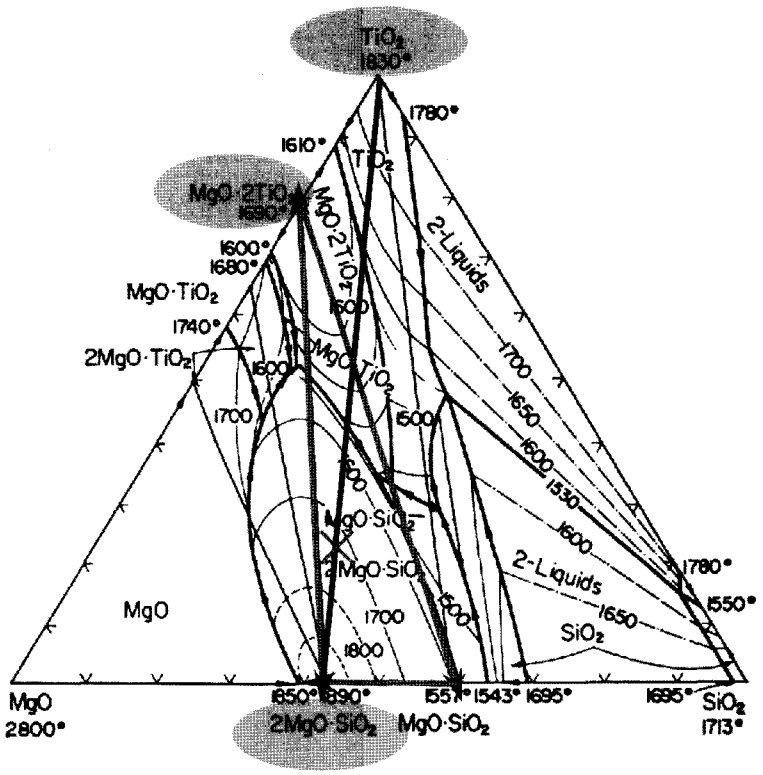

Fig. 9. Ternary phase diagram of MgO-SiO_2-TiO_2: Phase Diagrams for Ceramics No.723 by F. Massazza et al. (1958).[21]

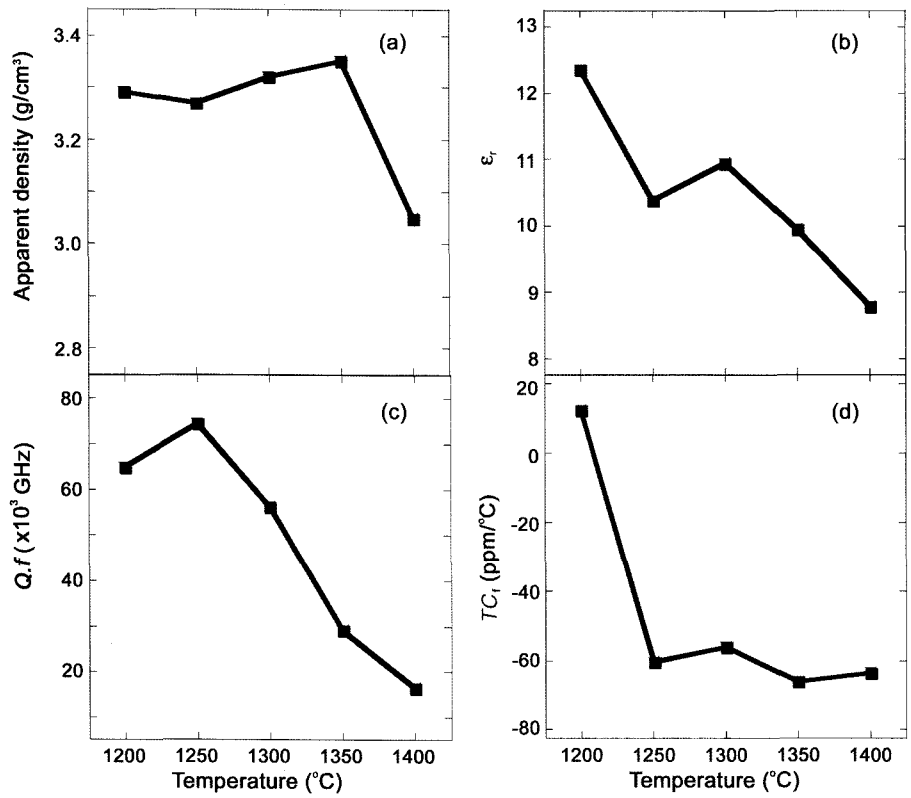

Fig. 10. Apparent density (a), quality factor (b), dielectric constant (c), the TC_f (d) of the Mg_2SiO_4 added 30 wt% TiO_2 ceramics as a function of the sintering temperature.

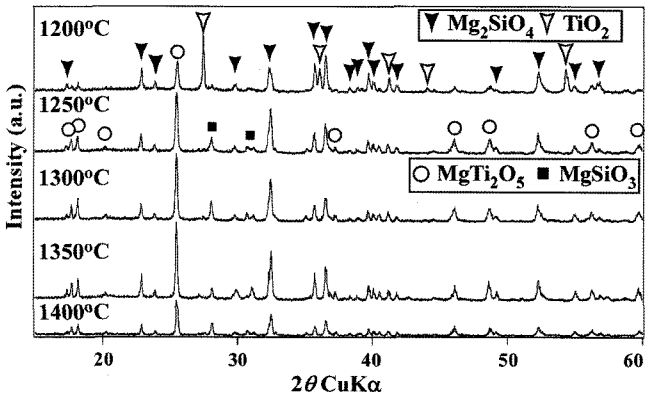

Fig. 11. XRPD patterns of the forsterite ceramics added 30 wt% rutile as a function of sintering temperature.

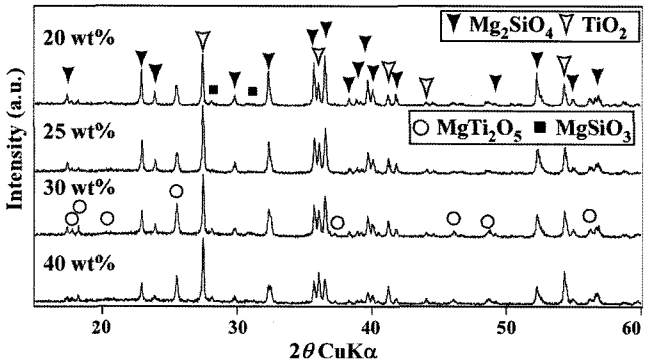

Fig. 12. XRPD patterns of the Mg_2SiO_4 added TiO_2 ceramics sintered at 1200 °C for 2 h.

tive TC_f of 450 ppm/ °C, as shown in XRPD pattern in Fig. 11. The TC_f changed abruptly from negative value to positive one with lowering sintering temperature, it shows 12.7 ppm/ °C for the sample sintered at 1200 °C. Although ε_r values shifts to high value with lowering sintering temperature, $Q \cdot f$ values are improved to over 70000 GHz as shown in Fig. 10(b) and (c). This shows the possibility of formation good dielectrics with TC_f=0 ppm/ °C and high $Q \cdot f$ at the sintering temperature between 1200 to 1250°C.

Fig. 12 shows XRPD patterns of the forsterite ceramics added 20 to 40 wt% rutile sintered at 1200°C. Residual rutile phases observed in all samples accompanying with $MgTi_2O_5$ and enstatite, which are the components of the compositional triangle. This means that rutile acts as sintering aid by means of reaction with forsterite. In the XRPD patterns, rutile and other secondary phases are increased with the amount of added rutile. The residual rutile acts the TC_f to improve near zero. Fig. 13 shows apparent density and dielectric properties of the samples sintered at 1200°C for 2 h as a function of rutile amount. The TC_f of forsterite ceramics added rutile increased linearly with amount of rutile addition as shown in Fig. 13(d). The TC_f changed from negative to positive values between 20 and 25 wt% addition of rutile. The TC_f showed 3.95 ppm/ °C in the case of 25 wt% addition of rutile. Although ε_r values shifts to high value with amount of rutile, the $Q \cdot f$ values also keep high value over the 60000 GHz as shown in Fig. 13(c) and (b), respectively. The increase of apparent density is attributed to addition of rutile with higher density (4.24 g/cm^3) than forsterite (3.22 g/ cm^3). It is inferred to have TC_f=0 ppm/ °C, ε_r=11 and $Q \cdot f$= 82000 GHz in the forsterite with 24 wt% rutile ceramic composite sintered at 1200°C for 2 h. Fig. 14 shows back scattered SEM photograph of the forsterite with 25 wt% rutile ceramic composite sintered at 1200°C for 2 h. The microstructure was composed by grains of forsterite (light gray grains) and rutile crystals (white grains) and densified in the

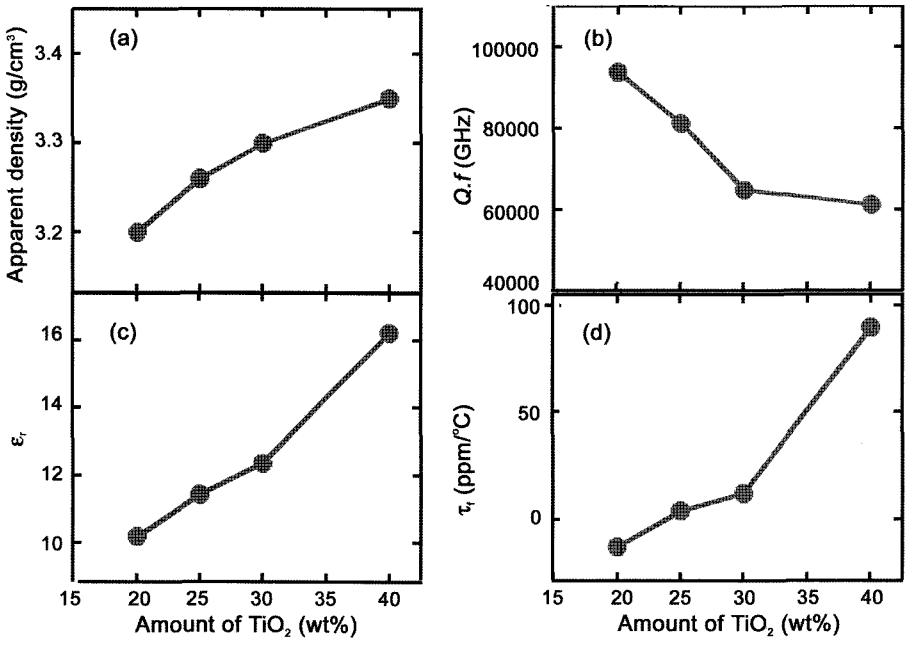

Fig. 13. Apparent density and microwave dielectric properties of the rutile doped forsterite ceramics sintered at 1200°C for 2 h as a function of rutile contents.

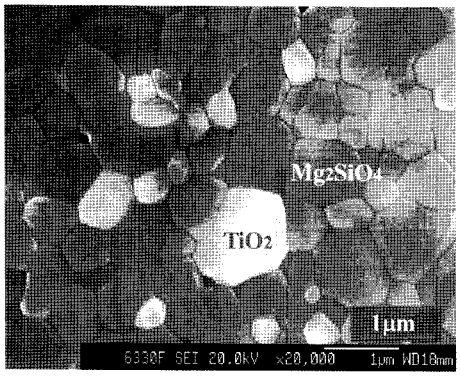

Fig. 14. A SEM micrograph of the Mg_2SiO_4 with 25 wt% TiO_2 ceramic composite sintered at 1200°C for 2 h.

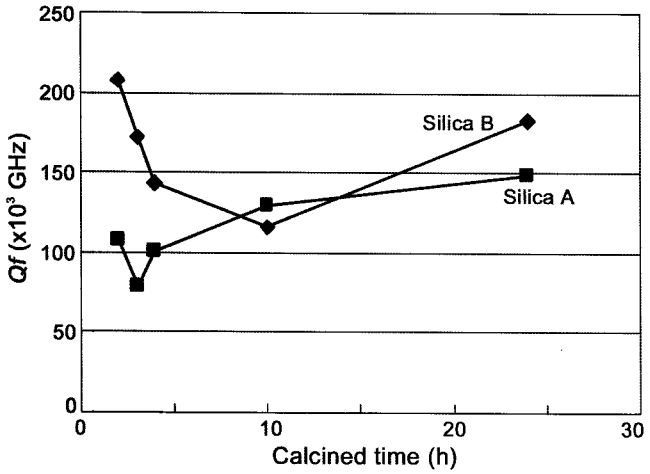

Fig. 15. $Q \cdot f$ values as a function of calcination time for specimens sintered at 1400°C for 2 h.

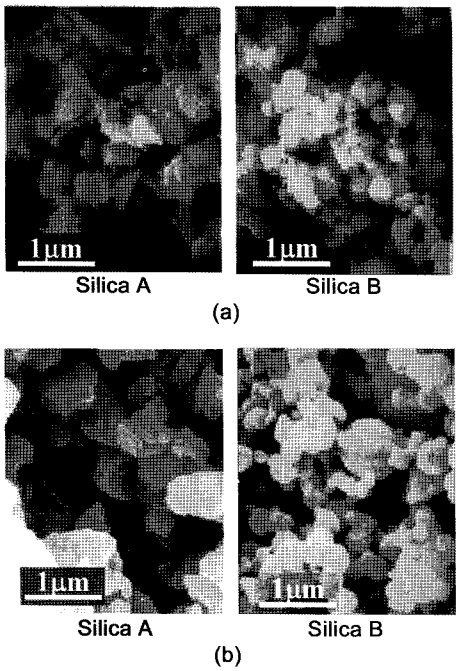

Fig. 16. SEM images of raw materials (a) and calcined samples at 1175°C for 24 h (b).

state of pore and glassy-phase free at grain boundaries. This seemed to be due to the enhanced sinterability by excess rutile addition.

3.3. Adjust the sintering conditions

Generally, synthesis of silicates is very difficult and needs many know how, because there are many synthesis conditions, that is, selection of raw materials with different phase, shape and size, and processing such as calcined, sintering conditions, press conditions and so on. We clarified the effects on the formation and properties by mean of different diffusion on the Si and Mg elements. Fig. 15 shows the $Q \cdot f$ of specimens sintered at 1400°C for 2 h as a function of calcination time: 2-24 h. The specimens were calcined at 1175°C for silica A with a crystalline form and a large grain size of 0.82 μm for SiO_2 raw material, and 1175°C for silica B with an amorphous form and a small size of 0.25 μm. The difference in crystalline form or grain size is clearly observed in Fig 16(a). The $Q \cdot f$ values changed markedly in the narrow calcination time range of 2 to 4 h and then moderately changed for calcination times over 10 h. In the case of silica A, the $Q \cdot f$ values of the sintered specimen calcined at 1175°C are decreased for calcination times of up to 4 h and then increased up to 24 h. On the other hand, in the case of silica B, the $Q \cdot f$ values of the sintered specimen calcined at 1175°C are also decreased for calcination times of up to 10 h and then increased up to 24 h. The reproduce of this tendency was confirmed by re-research and the reason was also clarified by the difference of diffusion on the Si and Mg ions as mentioned below.

Fig. 17 shows the apparent densities of samples sintered at 1400°C using silica A and silica B as a function of calcination

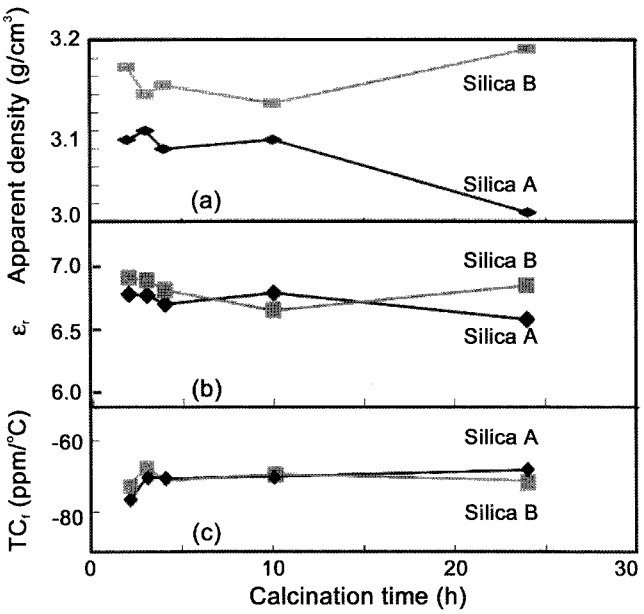

Fig. 17. Apparent densities (a), dielectric constant ε_r (b) and temperature coefficient of resonance frequency TC_f (c) of specimens sintered at 1400°C for 2 h as a function of calcination time.

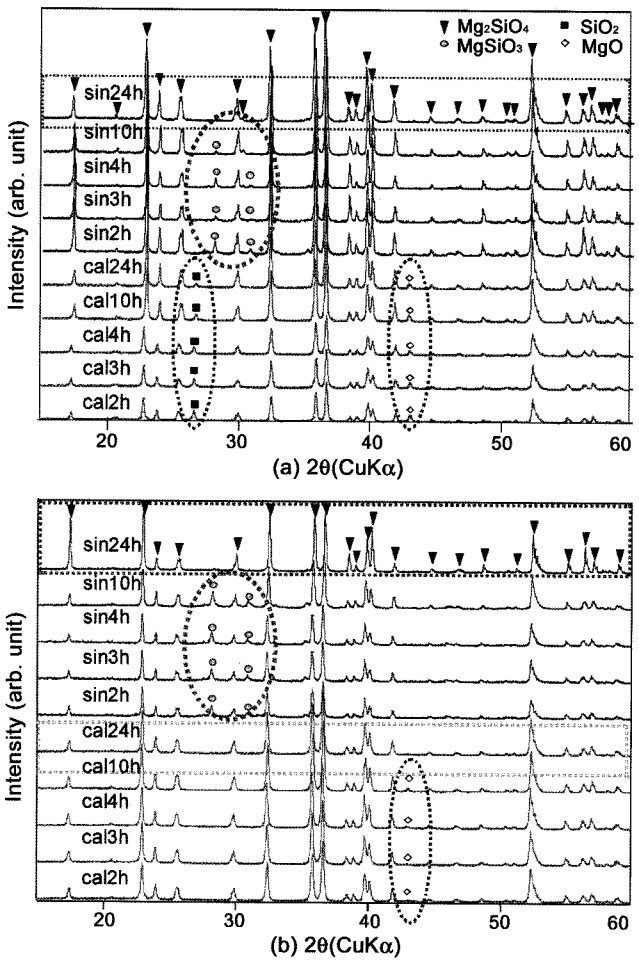

Fig. 18. XRPD patterns of powders prepared by using silica A (a) and silica B (b). The XRPD patterns shown below the half way point in (a) and (b) represent the difference in composition for powder samples calcined at 1175°C for 2, 3, 4, 10, and 24 h denoted as "cal *n* h", and those above the halfway point in (a) and (b) represent that for 1175°C calcined samples sintered at 1400°C for 2 h denoted as "sin *n* h".

time. In the case of silica A, the densities decreased from 3.10 to 3.01 g/cm^3 with increasing calcination time. On the other hand, in the case of silica B, the densities decreased up to 10 h and increased markedly to 3.19 g/cm^3 for the sample calcined for 24 h. Fig. 16(b) shows SEM images of forsterite powders prepared by calcining a mixture of magnesia and silica at 1175°C for 24 h. According to compare Fig. 16(a) with Fig. 16(b), the shape and size distribution of both silica A and silica B raw materials are maintained in calcined powder forsterite. This phenomenon depends on the reaction between silica and MgO. The reactions are carried out to maintain the shape and size through the diffusion of Mg ions from the MgO grain with a small size of 0.06 μm. As the size has a distribution, the change in grain size was not clarified. The spherical shape and wider size distribution of the powders (silica B) result in higher packing density, which contribute to the realization of the sintered pellet with higher apparent density as shown in Fig. 17(a). The high density of the sample calcined for 24 h brought a high $Q \cdot f$ of 180,000 GHz. Fig. 18(a) and (b) shows XRPD patterns of specimens prepared using silica A and silica B, respectively, which include two types of diffraction patterns for calcined and sintered specimens with different calcination times. The XRPD patterns for calcined powder are denoted by "cal *n* h" n=2, 3, 4, 10, 24. The sintered ceramic prepared using calcined powder "cal *n* h" is denoted by "sin *n* h". All ceramics were sintered at 1400°C for 2 h. All the crystalline XRPD patterns indicate that the ceramics are mainly composed of forsterite. The amount of enstatite ($MgSiO_3$) observed in sintered specimens prepared using silica A decreased with calcination time and the material almost disappeared at the calcination time of 24 h resulting in a single phase of forsterite as shown in Fig. 18(a), although the calcined samples include the unreacted raw materials: periclase (MgO) and quartz (SiO_2). The enstatite phase was also detected in the sintered specimen prepared using silica B as shown in Fig. 18(b). However, the tendency of a monotonic decrease in enstatite content with calcination time was not observed and the material suddenly almost disappeared at the time of 24 h. The calcined samples prepared using silica B with an amorphous form and fine grains are composed of only the unreacted raw material of MgO and resulted in a single phase of forsterite at the calcination time of 24 h. Until 10 h amorphous silicates may remain with MgO, which is not detected by XRPD analysis. However, the amount of unreacted raw materials was reduced using the amorphous silica with a spherical shape. It was clarified that $Q \cdot f$ values are affected by the amount of enstatite. Particularly, in the case of silica A, $Q \cdot f$ values increased as the amount of enstatite decreased between "sin 2 h" and "sin 10 h" as shown in Figs. 15 and 18(a). On the other hand in the case of silica B, $Q \cdot f$ decreased up to 10 h as the amount of enstatite increased between "sin 2 h" and "sin 10 h" as shown in Figs. 15 and 18(b). At "sin 24 h", when there was no trace of enstatite, the $Q \cdot f$ value increased. The effects of enstatite on the $Q \cdot f$ values of sintered ceramics have not yet been clarified, and they are under investigation.

Fig. 19 shows SEM images of specimens prepared using silica A sintered at 1400°C for 2 h as a function of calcination time. The sintered sample with high $Q \cdot f$ calcined for 24 h shows fine grains without small particles as shown in Fig. 19, silica A (e). The small particles might be MgO, which remains around the grains, suggesting that MgO diffusion during sintering is not completed. As calcination time increased, these small particles decreased in amount and finally disappeared at the time of 24 h in Fig. 19, silica A (e). Fig. 19, silica B shows a surface image of specimens prepared using amorphous silica B sintered at 1400°C for 2 h as a function of calcination time. Specimens calcined for 2 and 24 h with high $Q \cdot f$ show the same size and distribution of the particles, and the small particles also decreased in amount.

The ε_r values of all samples are between 6.5 and 7.0, and the TC_f values are between −67 and −77 ppm/ °C as shown

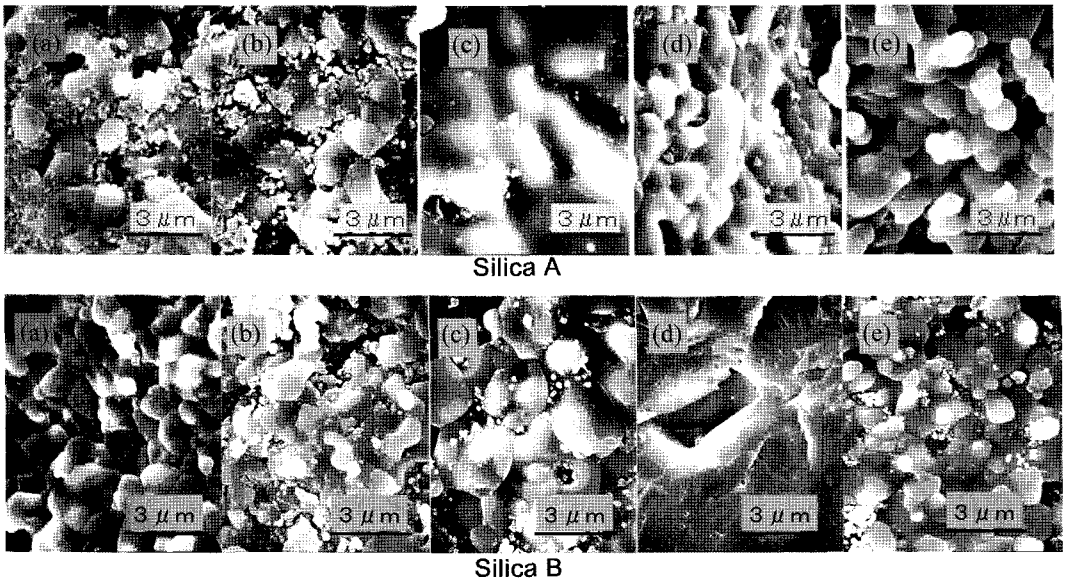

Fig. 19. Surface SEM images of specimens prepared by using silica A and silica B sintered at 1400°C for 2 h as a function of calcination time and at 1175°C for (a) 2, (b) 3, (c) 4, (d) 10, and (e) 24 h.

in Fig. 17(b) and (c), respectively. Moreover, when a specimen calcined at 1175°C for 24 h using amorphous silica B was sintered at 1450°C, the $Q \cdot f$ value was improved to 219100 GHz with ε_r=6.9 and TC_f=−68 ppm/°C.

4. Conclusions

Forsterite synthesized by using high purity law materials was improved $Q \cdot f$ to 240000 GHz.

Temperature coefficient of resonant frequency TC_f=−67 ppm/°C of forsterite was improved to near zero by adding rutile with positive TC_f of 450 ppm/°C, when it was sintered at 1200°C. Rutile plays two roles of sintering aid and adjusting TC_f. The sintering temperature of forsterite was reduced by 200°C from 1400°C. Trigger of this study was on the finding the sintering conditions with high density when it was sintered at 1200°C.

Difference of diffusion of SiO_4 and Mg ions brought different sintering conditions. Mg ions diffused into silica particle because of ion size difference. This phenomenon was clarified by the shape of calcined particles which were same shape with the raw silica. This calcined powder with spherical shape made dense and high Q forsterite ceramics.

Acknowlegements

A part of this work was supported by following projects: a Grant-in Aid for Science Research (B) and the NITECH 21st Century COE program "World Ceramics Center for Environmental Harmony" supported by Japanese Ministry of Education, Science and Culture; and NEDO foundation for matching fund.

REFERENCES

1. H. Ohsato, "Microwave Ceramics and Devices for Ubiquitous Computing*(in Japanese)*," Bull. Ceram. Soc. Jpn., **39**, 578 (2004).
2. H. Ohsato, "Research and Development of Microwave Dielectric Ceramics for Wireless Communications," *J. Ceram. Soc. Jpn.*, **113** [11] 703-11 (2005).
3. H. Ohsato, T. Tsunooka, A. Kan, Y. Ohishi, Y. Miyauchi, Y. Tohdo, T. Okawa, K. Kakimoto, and H. Ogawa, Key Eng. Mater., **269** 195 (2004).
4. R. C. Buchanan, Ceramic Materials for Electronics (Marcel Dekker, Inc., New York and Basel 1986), pp. 1-8.
5. H. Ohsato, M. Mizuta, T. Ikoma, Y. Onogi, S. Nishigaki, and T. Okuda, *J. Ceram. Soc. Jpn.*, **106** 178 (1998).
6. H. Ohsato, J. *Euro. Ceram. Soc.*, **21** 2703 (2001).
7. H. Ohsato, M. Suzuki, and K. Kakimoto, Ceram. Eng. and Sci. Pro., **26** [5] 135 (2005).
8. T. Okawa, K. Kiuchi, H. Okabe, and H. Ohsato, *Jpn. J. Appl. Phys.*, **40** 5779 (2001).
9. H. Ohsato, Y. Tohdo, K. Kakimoto, H. Okabe, and T. Okawa, *Ceram. Eng. Sci. Proc.*, **24** 75 (2003).
10. Y. Tohdo, K. Kakimoto, H. Ohsato, H. Yamada, and T. Okawa, *J. Euro. Ceram. Soc.*, **26** 2039 (2006).
11. H. Ohsato, T. Tsunooka, Y. Ohishi, Y. Miyauchi, M. Ando, and K. Kakimoto, *J. Kor. Ceram. Soc.*, **40** 350 (2003).
12. H. Ohsato, *Mater. Res. Soc. Symp. Proc.*, **833** 55 (2005).
13. T. Tsunooka, M. Andou, Y. Higashida, H. Sugiura, and H. Ohsato, *J. Eur. Ceram. Soc.*, **23** [14] 2573-78 (2003). ekker, Inc., (1986) pp.1-8.
14. T. Tsunooka, H. Sugiyama, K. Kakimoto, H. Ohsato, and

H. Ogawa, *J. Ceram. Soc. Jpn.*, Suppl., **112** 1637-40 (2004).
15. H. Ohsato, H. Kato, M. Mizuta, S. Nishigaki, and T. Okuda, *Jpn. J. Appl. Phys.*, **34** 5413 (1995).
16. T. Okamura and T. Kishino, *Jpn. J. Appl. Phys.*, **37** 5364-66 (1998).
17. M. Andou, T. Tsunooka, Y. Higashida, H. Sugiura, and H. Ohsato, Abstracts for Microwave Materials and Their Applications (York, UK, 2002) pp141.
18. M. Andou, K. Himura, T. Tsunooka, I. Kagomiya, and H. Ohsato, *Jpn. J. Appl. Phys.* **46** [9B] (2007), in press.
19. B. W. Hakki and P. D. Coleman, *IRE Trans. Microwave Theory & Tech., MTT-8*, 402 (1960).
20. Y. Kobayashi and M. Kato, *IEEE Trans. Microwave Theory & Tech., MTT-33*, 86 (1985).
21. Phase Diagrams for Ceramics No.723: Franco Massazza and Efisia Sirchia, Chim. Ind. (Milan), **40** 466 (1958).